

RS2V-L: Vehicle-Mounted LiDAR Data Generation from Roadside Sensor Observations

Ruidan Xing^{1,2,3}, Runyi Huang^{1,2,4}, Qing Xu^{1,2} and Lei He^{1,2,*}

Abstract—End-to-end autonomous driving solutions, which process multi-modal sensory data to directly generate refined control commands, have become a dominant paradigm in autonomous driving research. However, these approaches predominantly depend on single-vehicle data collection for model training and optimization, resulting in significant challenges such as high data acquisition and annotation costs, the scarcity of critical driving scenarios, and fragmented datasets that impede model generalization. To mitigate these limitations, we introduce RS2V-L, a novel framework for reconstructing and synthesizing vehicle-mounted LiDAR data from roadside sensor observations. Specifically, our method transforms roadside LiDAR point clouds into the vehicle-mounted LiDAR coordinate system by leveraging the target vehicle’s relative pose. Subsequently, high-fidelity vehicle-mounted LiDAR data is synthesized through virtual LiDAR modeling, point cloud classification, and resampling techniques. To the best of our knowledge, this is the first approach to reconstruct vehicle-mounted LiDAR data from roadside sensor inputs. Extensive experimental evaluations demonstrate that incorporating the generated data into model training—complementing the KITTI dataset—enhances 3D object detection accuracy by over 30% while improving the efficiency of end-to-end autonomous driving data generation by more than an order of magnitude. These findings strongly validate the effectiveness of the proposed method and underscore its potential in reducing dependence on costly vehicle-mounted data collection while improving the robustness of autonomous driving models.

I. INTRODUCTION

End-to-end autonomous driving models, exemplified by Tesla FSD, aim to fully neuralize core autonomous driving algorithms[1], significantly reducing the reliance on manually coded rule-based logic. These models have gradually become the mainstream trend in autonomous driving technology[2], [3]. However, current end-to-end autonomous driving systems still face several challenges, including high data collection and annotation costs, scarcity of high-value driving scenarios, and difficulties in effectively mining such scenarios[4]. Additionally, data silos arise as individual automakers restrict data loops to their own vehicle models,

limiting cross-vehicle and cross-scenario adaptability and hindering model generalization.

To address these challenges, we propose a novel method to reconstruct vehicle-mounted LiDAR data from roadside sensor data, leveraging roadside sensors to generate high-precision dynamic and static 3D scene reconstructions. This enables the creation of sensor data adaptable to different vehicle models and sensor configurations across various automakers. Our method offers several key advantages: (1) All-weather, all-operation condition adaptation, ensuring stable performance across diverse environments and road conditions; (2) Support for arbitrary vehicle models and sensor configurations, enhancing model adaptability; (3) Low-cost, high-efficiency data generation, significantly reducing the cost of autonomous driving data collection and annotation; (4) Consistency between generated and real-world data, effectively mitigating the Sim2Real domain adaptation issue[5], thereby improving training stability and generalization.

Specifically, our approach first models vehicle-mounted LiDAR sensors based on roadside LiDAR point clouds, incorporating the relative pose of the target vehicle within the scene. The roadside LiDAR data is then mapped to the vehicle-mounted LiDAR coordinate system. Subsequently, for each virtual LiDAR ray, a plane fitting approach is applied within its cone of vision using the roadside LiDAR point cloud. The intersection of the ray and the fitted plane is designated as the corresponding LiDAR point. If both ground points and non-ground points exist within the ray’s field of view, the non-ground points are prioritized for plane fitting to determine the final LiDAR sampling point, ensuring data accuracy and consistency.

Our Main Contributions:

- The first method to reconstruct vehicle-mounted LiDAR sensor data from roadside sensor data.
- A novel LiDAR sampling and modeling approach that eliminates the Sim2Real adaptation issue, enhancing data realism and consistency.
- Comprehensive experiments validating the effectiveness of the proposed method, demonstrating its capability to efficiently generate end-to-end autonomous driving training data for different vehicle models.

II. RELATED WORK

The rapid advancement of autonomous driving research is fundamentally driven by the availability of large-scale, high-quality datasets. However, the high cost associated with collecting point cloud data, coupled with severe data

arXiv:2503.07085v1 [cs.RO] 10 Mar 2025

*Corresponding author helei2023@tsinghua.edu.cn

¹School of Vehicle and Mobility, Tsinghua University, Beijing, 100084, China.

²State Key Laboratory of Intelligent Green Vehicle and Mobility, Tsinghua University, Beijing, 100084, China.

³School of Instrumentation and Optoelectronic Engineering, BeiHang University, Beijing, 100191, China.

⁴Department of Automation, Tsinghua University, Beijing, 100084, China.

This study is supported by the National Key R&D Program of China, Project "Development of Large Model Technology and Scenario Library Construction for Autonomous Driving Data Closed-Loop" (Grant No. 2024YFB2505501).

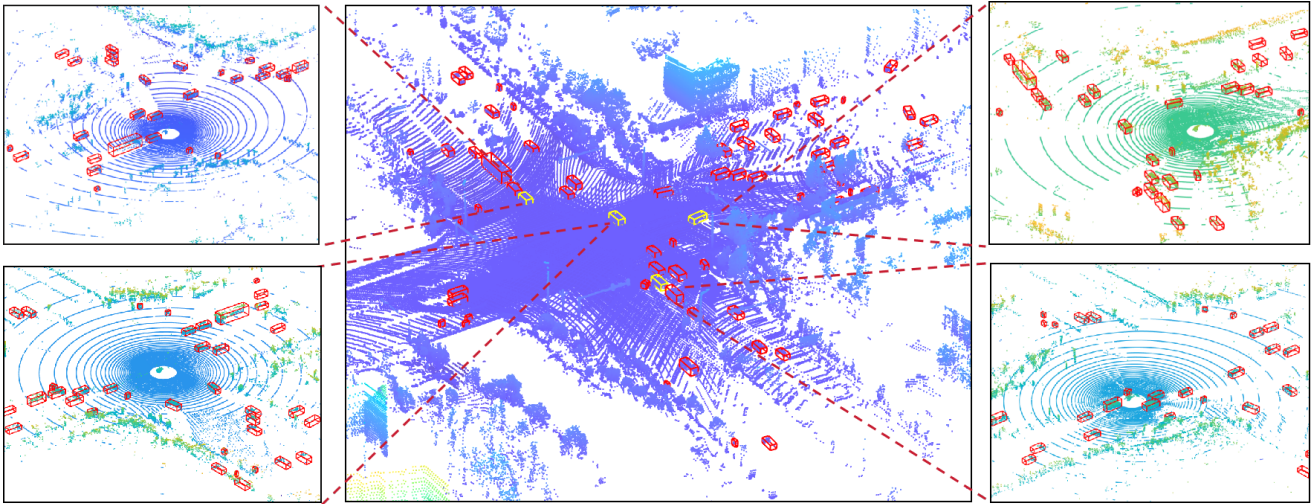


Fig. 1. The proposed method generates vehicle-mounted LiDAR data for the four corresponding vehicles in the scene based on roadside LiDAR observations. The central section of the figure illustrates the data collected by the roadside LiDAR, while the left and right sections depict the vehicle-mounted LiDAR data for the vehicles highlighted within the yellow annotation boxes.

silos, poses significant challenges for researchers in acquiring sufficient real-world data for training deep learning models. Consequently, generating reliable point cloud data for end-to-end autonomous driving training has emerged as a key research focus in recent years. Existing approaches for point cloud data generation can be broadly categorized into two main types: real-vehicle-based generation and environment simulation.

A. Real-Vehicle-Based Generation

Acquiring datasets from real vehicles is the most intuitive approach, and the release of various large-scale autonomous driving datasets has significantly propelled research in this field. For instance, SYNTHIA [6] and Cityscapes [7] primarily provide 2D annotations for images, whereas datasets such as KITTI [8], nuScenes [9], and Waymo [10] offer multi-modal data, including camera images and LiDAR point clouds, thereby serving as valuable resources for autonomous driving perception tasks. However, the collection and annotation processes are costly and labor-intensive, and these datasets often fail to comprehensively cover rare and complex long-tail scenarios. This limitation has motivated researchers to explore alternative data generation methodologies.

Early approaches for point cloud generation predominantly relied on Range Image Representation. However, such methods suffer from accuracy limitations in large-scale and complex environments. Caccia et al. [11] proposed a deep generative model-based method, where LiDAR scans were projected onto a 2D spherical point map, followed by the application of generative adversarial networks (GANs) and variational autoencoders (VAEs) for unconditional LiDAR point cloud generation. To enhance the quality of the generated 2D signals, absolute position information was incorporated. Building upon this foundation, Zyrianov et al. [12] introduced LiDARGen, which employs a point-based diffusion model for random denoising in an equirectangular projection

view, thereby improving the realism and scalability of point cloud generation. However, the range image representation is inherently ego-centric, often failing to preserve the curved structures within LiDAR data and exhibiting limitations in recovering point clouds at certain viewing angles.

To address these shortcomings, UltraLiDAR [13] leverages a Bird’s Eye View (BEV) voxel grid representation, enabling the encoding of geometric structures and occlusion relationships within point clouds to facilitate point cloud completion, generation, and manipulation. While UltraLiDAR excels in completing sparse point clouds, it lacks the flexibility needed for generating point clouds from arbitrary perspectives. LiDARDM [14] further advances the field by integrating implicit diffusion models with physical simulations to generate temporally consistent 4D LiDAR sequences, which are particularly useful for training and evaluating autonomous driving models. However, these methods predominantly rely on vehicle-mounted LiDAR data. Due to the height constraints of the vehicle itself and occlusions within dense traffic environments, such methods struggle to overcome limitations in field-of-view coverage.

In contrast, data generation based on roadside sensors is inherently free from vehicle height constraints and occlusion issues, allowing for the acquisition of more comprehensive point cloud information [15]. Accordingly, our proposed method leverages real-world roadside LiDAR data, which not only preserves the curved structural characteristics of point cloud data but also mitigates mutual occlusion effects between vehicles, thereby providing a more complete and reliable dataset for autonomous driving applications.

B. Environmental Simulation

An alternative approach to point cloud generation involves synthesizing LiDAR data within simulation environments, such as CARLA [16] and Gazebo [17], which utilize ray-casting techniques to simulate LiDAR sensing. These plat-

forms emit rays from a virtual sensor origin and compute their intersections with geometric surfaces to construct point clouds. CARLA [16] and AirSim [18] provide high-fidelity environments populated with both static (e.g., buildings, trees) and dynamic (e.g., vehicles, pedestrians) objects, enabling the generation of structured point clouds via virtual LiDAR sensors. However, the reliance on predefined 3D assets inherently constrains scene diversity and limits the ability to accurately replicate complex real-world dynamics. Furthermore, the well-documented *sim-to-real* gap poses a significant challenge, impeding the direct transferability of models trained on synthetic data to real-world scenarios.

To mitigate *sim-to-real* discrepancies, various data-driven approaches have been proposed. For instance, LiDARSim [19] leverages deep learning techniques to correct simulation artifacts, while NeRF-based methods [20][21] enhance the fidelity of asset reconstruction, refining the alignment between synthetic and real point cloud distributions. Despite these advancements, such methods remain dependent on simulation frameworks or reconstructed 3D assets, making it difficult to fully eliminate *sim-to-real* inconsistencies. Additionally, many of these techniques require substantial amounts of real-scanned data for fine-tuning, leading to considerable data acquisition costs.

In contrast, this study departs from conventional simulation-based paradigms by leveraging real-world roadside sensor data to directly generate LiDAR point clouds. This approach not only reduces *sim-to-real* discrepancies but also enhances model generalization in real-world environments, overcoming the limitations associated with synthetic data generation.

III. METHOD

This section provides a detailed exposition of the technical implementation of the RS2V-L system. Specifically, Section 3.1 presents the coordinate system transformation and data alignment process, which maps roadside LiDAR data to the vehicle-mounted coordinate frame based on real-time pose estimation. Section 3.2 introduces the methodology for generating virtual LiDAR data at the vehicle end. To achieve accurate scene reconstruction, we employ Patchwork++ [22] for semantic segmentation of object and ground point clouds. The segmented non-ground and ground point clouds are modeled separately, facilitating the synthesis of vehicle-mounted LiDAR point clouds through a virtual radar ray-tracing model. The overall architecture of the proposed method is illustrated in Fig. 2.

A. Roadside-to-Vehicle Coordinate System Transformation and Data Alignment

Let the original roadside LiDAR point cloud dataset be denoted as Q_w , with all point coordinates expressed in the world coordinate system $O_w-x_wy_wz_w$. This dataset is semantically annotated with scene objects, including their categories, three-dimensional geometric dimensions, centroid coordinates X_w in the world coordinate system, and corresponding rotation vectors θ_w .

To reconstruct vehicle-mounted LiDAR data, we first identify a target vehicle of interest from the annotated dataset. Let its pose parameters in the world coordinate system be given by (X_{wc}, θ_{wc}) . Utilizing the relative transformation ΔT between the vehicle-mounted LiDAR and the target vehicle, we establish the vehicle-mounted LiDAR coordinate system $O_c-x_cy_cz_c$. Following the standard coordinate system conventions of the KITTI dataset, the z -axis is defined as perpendicular to the ground and oriented upward, the x -axis points forward in the vehicle’s direction of motion, and the y -axis extends laterally to the left, aligning with the vehicle’s coordinate frame.

Based on this transformation framework, we derive a rigid-body transformation model that maps the roadside LiDAR data from the world coordinate system to the vehicle-mounted LiDAR coordinate system. The mathematical formulation of this transformation is given by:

$$R = \text{Rodrigues}(\theta_{wc})^{-1} \quad (1)$$

$$T = -RX_{wc} - \Delta T \quad (2)$$

where $\text{Rodrigues}(\cdot)$ represents the Rodrigues rotation formula.

Building upon the rigid-body transformation model, precise alignment of the point cloud data from the global coordinate system to the vehicle-mounted radar coordinate system is achieved, yielding the transformed point cloud Q_c in the vehicle-mounted radar frame. Simultaneously, corresponding transformations are applied to the annotation information to ensure consistency across coordinate systems. Throughout this process, the object’s category and geometric dimensions remain unchanged, while its pose (X_c, θ_c) in the vehicle-mounted radar coordinate system is computed using the following expressions:

$$X_c = RX_w + T \quad (3)$$

$$\theta_c = \text{InvRodrigues}(R \cdot \text{Rodrigues}(\theta_w)) \quad (4)$$

B. Vehicle-Mounted LiDAR Data Generation Method

To facilitate accurate point cloud synthesis, we first establish a virtual LiDAR model. Based on the LiDAR parameters used in the KITTI dataset, we construct a vehicle-mounted virtual LiDAR system within a spherical coordinate framework. The system operates within a sensing range of 0.5 m to 100 m, covering a horizontal field of view of $[0, 360^\circ]$ and a vertical field of view spanning $[88^\circ, 114^\circ]$. The horizontal and vertical resolutions are defined by m and k discrete lines, respectively, resulting in a total of $n = m \times k$ rays per scan cycle.

The virtual LiDAR emits a set of rays, denoted as L , originating from the center of the spherical coordinate system and propagating in all directions. Each individual ray is indexed as l_{ij} , where $i = 0, 1, 2, \dots, m-1$ represents the horizontal division index, and $j = 0, 1, 2, \dots, k-1$ represents the vertical division index. The horizontal azimuth angle φ_{ij} and vertical elevation angle θ_j for the (i, j) -th ray are

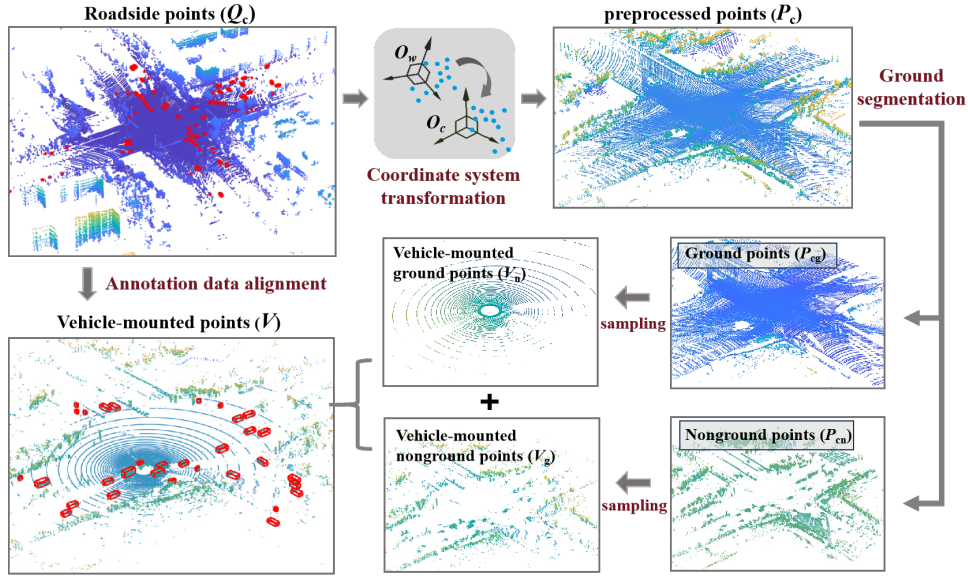


Fig. 2. The overall technical architecture of RS2V-L.

computed as follows:

$$\begin{cases} \varphi_{ij} = \frac{i}{m} \times 360^\circ \\ \theta_j = 88^\circ + \frac{j}{k} \times 26^\circ \end{cases} \quad (5)$$

Subsequently, the complete ray set L is defined as $L = \{l_{ij}(\varphi_{ij}, \theta_j) : i = 0, 1, 2, \dots, m-1; j = 0, 1, 2, \dots, k-1\}$. Taking the origin of the spherical coordinate system as the vertex and each ray in L as its central axis, a corresponding cone-shaped view frustum is constructed. The angular resolution of the LiDAR in the vertical direction, given by $(k/26)^\circ$, determines the cone angle of each frustum. This results in a collection of view frustums denoted as $W = \{w_{ij} : i = 0, 1, 2, \dots, m-1; j = 0, 1, 2, \dots, k-1\}$, where each individual frustum w_{ij} is associated with its corresponding ray l_{ij} , as illustrated in Fig. 3.

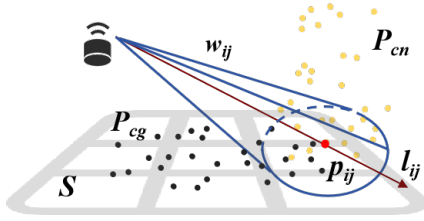


Fig. 3. Schematic Representation of LiDAR Ray l_{ij} and Corresponding View Frustum w_{ij} .

Upon the completion of the vehicle-mounted virtual LiDAR model construction, pre-processing and ground segmentation operations are applied to the input point cloud data Q_c . Let the initial point cloud be represented as $Q_c = \{q_1, q_2, \dots, q_N\}$, which is subsequently transformed into its spherical coordinate representation. Based on the predefined sensing range of the virtual LiDAR model, points falling outside this range are discarded, yielding the pre-processed

point set $P_c = \{p_1, p_2, \dots, p_N\}$, as depicted in the upper-right corner of Fig. 2. Each point in this set is expressed as $p_s = (\rho_s, \varphi_s, \theta_s)$.

Next, Patchwork++ [22] is employed to perform ground segmentation on P_c , partitioning it into a non-ground point cloud P_{cn} and a ground point cloud P_{cg} , as illustrated in the lower-right corner of Fig. 2. For any point p_i in the non-ground point cloud P_{cn} , its corresponding view frustum is determined based on its polar angle θ_i and azimuth angle φ_i . Within each frustum, plane fitting is performed separately for the contained point cloud. In contrast, the ground point cloud P_{cg} undergoes a global plane fitting process via the least-squares method, as shown in Fig. 3.

To associate each non-ground point $p_i \in P_{cn}$ with its corresponding ray and view frustum, its indices (i, j) are determined based on its polar and horizontal angular divisions as follows:

$$\begin{cases} i = \text{round}(\frac{m}{360^\circ} \varphi_i) \bmod m \\ j = \text{round}(\frac{k}{26^\circ} \theta_i) \bmod k \end{cases} \quad (6)$$

Denote the point set corresponding to the ray l_{ij} and its associated view frustum w_{ij} as P_{ij} , where $P_{ij} = \{p_s \in P \mid i = \text{round}(m\varphi_i/360^\circ) \bmod m, j = \text{round}(k\theta_i/26^\circ) \bmod k\}$. In scenarios where the roadside point cloud is relatively sparse, to ensure sufficient density in the generated non-ground point cloud, the angular range of the view frustum can be expanded to approximately 2–3 times its original value, thereby increasing the number of points encompassed within each frustum. For each non-empty point set P_{ij} , a plane S_{ij} is fitted using the least-squares method. Subsequently, based on the ray-tracing model, the intersection point p_{ij} between the corresponding ray l_{ij} and the fitted plane S_{ij} is computed. The resulting intersection point p_{ij} serves as the sampling point of the vehicle-mounted virtual LiDAR along the direction $(\varphi_{ij}, \theta_{ij})$. All valid intersection points are aggregated into

a set V_n , which constitutes the vehicle-mounted non-road surface point cloud data.

For the ground point cloud P_{cg} , a global plane fitting approach is employed to derive the fitted ground plane S . To refine the selection of valid sampling points, rays l_{ij} that contain non-ground points within their respective view frustums but lack ground points are filtered out. For the remaining rays, their intersection points p_{ij} with the plane S are computed. All valid intersection points are then collected to form the set V_g , representing the vehicle-mounted road surface point cloud data. Finally, merging V_n and V_g results in the complete vehicle-mounted LiDAR point cloud dataset V , as illustrated in the lower-left corner of Fig. 2.

IV. EXPERIMENT

In this study, experiments are conducted using a roadside multi-sensor dataset independently collected by our team. This dataset is acquired through continuous data collection by four 128-line LiDAR sensors deployed at intersections, encompassing a total of 531 frames captured across 50 distinct time periods, including morning and evening rush hours, off-peak hours, and nighttime. Leveraging this dataset, we employ the RS2V-L system to generate 6000 frames of vehicle-mounted point cloud data, covering more than 1000 unique vehicles. On average, each time period captures point cloud data for over 20 different vehicles. The RS2V-L system not only enhances dataset acquisition efficiency by more than an order of magnitude but also significantly enriches data diversity. The generation results are illustrated in Fig. 1.

To assess the effectiveness of the data generated by the RS2V-L method in improving model training, we randomly select 4000 frames for experimentation. The dataset is partitioned into a training set comprising 3000 frames and a test set consisting of 1000 frames. A 3D object detection benchmarking platform is constructed based on OpenPCDet [23], with the KITTI dataset [8] serving as the baseline for comparison. A comprehensive evaluation is conducted from two perspectives: (1) the overall performance enhancement of the model and (2) the specific improvements in complex traffic scenarios, such as densely populated intersections with high traffic flow.

A. Overall Model Performance Improvement

To evaluate the impact of the generated data on model performance, a comparative experiment was designed. The control group was trained solely on the KITTI dataset (KITTI: 3712), whereas the experimental group incorporated both the KITTI dataset and an additional 3000 frames of generated data (KITTI: 3712, RS2V-L: 3000) for enhanced training. All training procedures were conducted using the PointPillar [24] model, and vehicle detection performance was assessed on the KITTI validation set. The core evaluation metrics included average precision (AP) and AP_R40 across three key aspects: Bird’s-Eye View (BEV) bounding boxes, 3D bounding boxes, and the target orientation estimation (AOS).

As summarized in TABLE I, the experimental group consistently outperformed the control group across all key metrics. Specifically, the AP values for BEV, 3D, and AOS in the experimental group exhibited a significant increase compared to the control group. Furthermore, improvements were also observed in the AP_R40 metric, indicating that the dataset generated using the RS2V-L method enhances the model’s generalization capabilities across diverse scenarios and driving conditions. These results demonstrate that the RS2V-L framework serves as an effective tool for data augmentation and model optimization, thereby improving the robustness and reliability of autonomous driving perception models.

TABLE I
EVALUATION OF KITTI DATASET PERFORMANCE UNDER DIFFERENT TRAINING DATA CONFIGURATIONS

Indicator	Metric	Results	
		KITTI	KITTI+RS2V-L
AP	BEV	60.9018	78.0783
	3D	35.7113	65.4087
	AOS	66.89	72.21
AP_R40	BEV	61.4127	80.8127
	3D	32.8083	65.3331
	AOS	66.89	72.34

B. Optimization for Complex Scenarios

To evaluate the effectiveness of the RS2V-L-generated data in enhancing model performance under complex scenarios, as well as to assess its applicability for data collection in extreme conditions, this study integrates the generated dataset into the KITTI training set for joint training. The evaluation focuses on the performance of models tested on the generated vehicle-mounted LiDAR data collected in intersection scenarios. The experimental setup remains consistent with Experiment A, and a comparative study is conducted as follows:

TABLE II
EVALUATION OF RS2V-L DATASET PERFORMANCE UNDER DIFFERENT TRAINING DATA CONFIGURATIONS

Indicator	Metric	Results	
		KITTI	KITTI+RS2V-L
AP	BEV	1.30	34.98
	3D	0.01	28.65
	AOS	47.47	44.62
AP_R40	BEV	0.35	31.96
	3D	0.01	25.31
	AOS	44.74	45.71

According to the test results presented in TABLE II, the average precision (AP) of the 3D detection boxes in the experimental group reaches 28.65, a substantial improvement compared to the mere 0.01 observed in the control group. Similarly, the accuracy of the Bird’s-Eye-View (BEV) detection boxes has also exhibited a significant enhancement. Fig.4 illustrates the visualization results of the experiment, demonstrating that the model trained on the mixed dataset, which incorporates the generated data, achieves a markedly

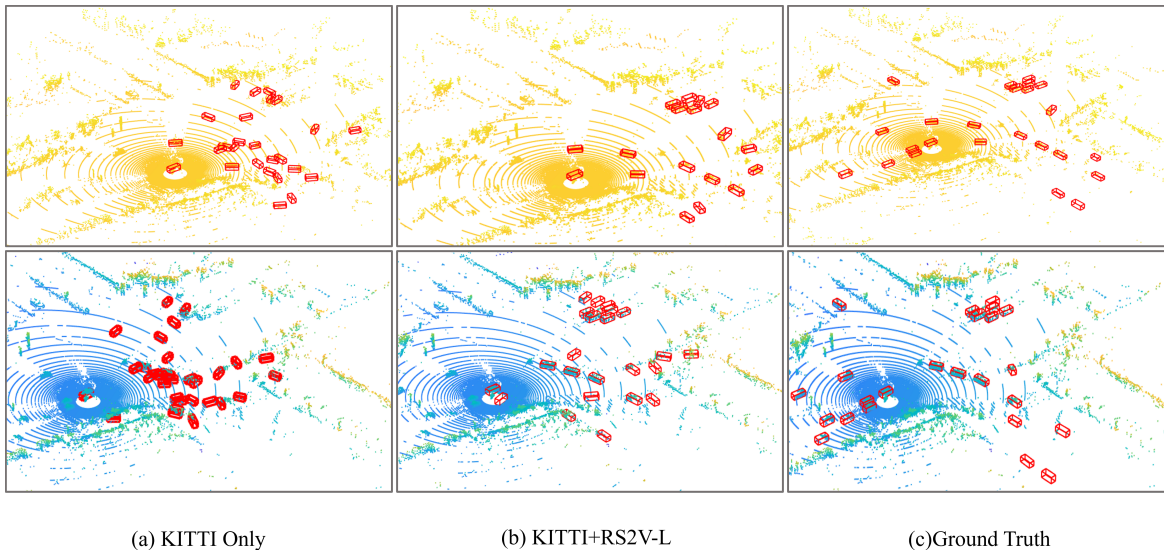


Fig. 4. A comparative analysis of the experimental results is presented as follows: (a) illustrates the detection outcomes obtained after training exclusively on the KITTI dataset, where bounding boxes in densely packed vehicle regions exhibit significant clutter and are highly susceptible to misclassification. (b) displays the results following training on both our generated dataset and the KITTI dataset, demonstrating a substantial enhancement in object separation in real-world test scenarios. (c) represents the ground truth annotations. Compared to (a), (b) highlights the effectiveness of our generated dataset in alleviating the challenges associated with dense object occlusion in vehicle-mounted LiDAR datasets, thereby improving detection accuracy and robustness in complex traffic environments.

improved object-detection capability. These findings underscore that the RS2V-L-generated data effectively enhances the model’s ability to interpret complex scenarios, thereby improving its performance in object detection under such conditions. The RS2V-L framework proposed in this study leverages 531 frames of roadside LiDAR data to generate 6000 frames of vehicle-mounted LiDAR data, achieving a more than tenfold increase in data collection efficiency. Furthermore, the effectiveness of the RS2V-L-generated data in improving model performance is systematically validated through two sets of comparative experiments.

In the overall performance evaluation, the model trained with the augmented dataset, which incorporates the generated data, consistently outperforms the model trained solely on the KITTI dataset across multiple key metrics, including Bird’s-Eye-View (BEV), 3D detection, and the Angle of Object Sighting (AOS). Specifically, the BEV metric improves from 60.91 to 78.09, reflecting a 28-percentage-point increase; the 3D detection accuracy rises from 35.71 to 65.41, marking an 83-percentage-point enhancement; and the AOS metric increases from 66.89 to 72.71, representing an 8-percentage-point gain. In the complex scenario evaluation, particularly in intersection environments, the model trained with the augmented dataset significantly surpasses the baseline model trained solely on KITTI data in both 3D detection and BEV accuracy, demonstrating its robustness in handling challenging traffic conditions. In summary, the RS2V-L-generated data not only enhances the overall model performance but also substantially improves its effectiveness in complex and highly dynamic scenarios. This approach offers significant value for augmenting vehicle-mounted LiDAR datasets and facilitating data collection in extreme driving conditions.

V. CONCLUSIONS

This paper presents the RS2V-L method, which effectively reconstructs and synthesizes vehicle-mounted LiDAR data from roadside sensor observations, offering an efficient and cost-effective data generation paradigm for autonomous driving applications. Experimental evaluations demonstrate that the data generated by RS2V-L not only significantly enhances the overall performance of autonomous driving models but also exhibits remarkable adaptability in complex environments, such as intersections.

In contrast to conventional vehicle-mounted data acquisition approaches, RS2V-L capitalizes on the "god’s eye view" advantage of roadside sensors to mitigate vehicle-to-vehicle occlusion while addressing domain adaptation challenges between simulated and real-world data. Furthermore, this method accommodates arbitrary vehicle models and sensor configurations, ensuring broad applicability across diverse autonomous driving scenarios.

Future research will focus on further optimizing the RS2V-L framework, expanding its applicability to a wider range of scenarios and sensor modalities, and integrating multi-modal data generation techniques. These advancements aim to provide more comprehensive support for the continued development of autonomous driving technology.

REFERENCES

- [1] L. Chen, P. Wu, K. Chitta, et al., "End-to-end autonomous driving: Challenges and frontiers," *IEEE Trans. Pattern Anal. Mach. Intell.*, 2024.
- [2] T. H. Wang, A. Maalouf, W. Xiao, et al., "Drive anywhere: Generalizable end-to-end autonomous driving with multi-modal foundation models," in *Proc. 2024 IEEE Int. Conf. Robot. Autom. (ICRA)*, IEEE, 2024, pp. 6687-6694.

- [3] Lu, Siyi, et al. "Hierarchical end-to-end autonomous driving: Integrating bev perception with deep reinforcement learning." arXiv preprint arXiv:2409.17659, 2024.
- [4] M. Pitropov, et al., "Canadian adverse driving conditions dataset," *Int. J. Robot. Res.*, vol. 40, no. 4-5, pp. 681-690, 2021.
- [5] A. Kadian, et al., "Sim2real predictivity: Does evaluation in simulation predict real-world performance?," *IEEE Robot. Autom. Lett.*, vol. 5, no. 4, pp. 6670-6677, 2020.
- [6] L. G. Ros, J. Materzynska, D. Vazquez, and A. M. Lopez, "The SYNTHIA dataset: A large collection of synthetic images for semantic segmentation of urban scenes," in *Proc. IEEE Conf. Comput. Vis. Pattern Recognit.*, 2016, pp. 3234-3243.
- [7] M. Cordts, M. Omran, S. Ramos, et al., "The Cityscapes dataset for semantic urban scene understanding," in *Proc. IEEE Conf. Comput. Vis. Pattern Recognit.*, 2016, pp. 3213-3223.
- [8] A. Geiger, P. Lenz, and R. Urtasun, "Are we ready for autonomous driving? The KITTI vision benchmark suite," in *Proc. IEEE Conf. Comput. Vis. Pattern Recognit.*, IEEE, 2012, pp. 3354-3361.
- [9] H. Caesar, V. Bankiti, A. H. Lang, et al., "nuScenes: A multimodal dataset for autonomous driving," in *Proc. IEEE/CVF Conf. Comput. Vis. Pattern Recognit.*, 2020, pp. 11621-11631.
- [10] P. Sun, H. Kretschmar, X. Dotiwala, et al., "Scalability in perception for autonomous driving: Waymo open dataset," in *Proc. IEEE/CVF Conf. Comput. Vis. Pattern Recognit.*, 2020, pp. 2446-2454.
- [11] L. Caccia, H. v. Hoof, A. Courville, and J. Pineau, "Deep generative modeling of LiDAR data," in *Proc. IEEE/RSJ Int. Conf. Intell. Robots Syst. (IROS)*, 2019, pp. 5034-5040.
- [12] V. Zyrianov, X. Zhu, and S. Wang, "Learning to generate realistic LiDAR point cloud," in *Proc. Eur. Conf. Comput. Vis. (ECCV)*, 2022, pp. 17-35.
- [13] Y. Xiong, W. C. Ma, J. Wang, and R. Urtasun, "Learning compact representations for LiDAR completion and generation," in *Proc. IEEE/CVF Conf. Comput. Vis. Pattern Recognit.*, 2023.
- [14] V. Zyrianov, H. Che, Z. Liu, and S. Wang, "LiDAR-DM: Generative LiDAR simulation in a generated world," in *Proc. IEEE Int. Conf. Robot. Autom. (ICRA)*, 2025.
- [15] B. Gao, J. Liu, H. Zou, J. Chen, L. He, and K. Li, "Vehicle-road-cloud collaborative perception framework and key technologies: A review," *IEEE Trans. Intell. Transp. Syst.*, vol. 25, no. 12, pp. 19295-19318, Dec. 2024.
- [16] A. Dosovitskiy, G. Ros, F. Codevilla, A. Lopez, and V. Koltun, "CARLA: An open urban driving simulator," in *Proc. 1st Annu. Conf. Robot Learn.*, 2017, pp. 1-16.
- [17] N. Koenig and A. Howard, "Design and use paradigms for Gazebo, an open-source multi-robot simulator," in *Proc. IEEE/RSJ Int. Conf. Intell. Robots Syst. (IROS)*, vol. 3, IEEE, 2004, pp. 2149-2154.
- [18] S. Shah, D. Dey, C. Lovett, and A. Kapoor, "AirSim: High-fidelity visual and physical simulation for autonomous vehicles," in *Proc. Field Service Robot. (FSR)*, 2017.
- [19] S. Manivasagam, S. Wang, K. Wong, et al., "LiDARSim: Realistic LiDAR simulation by leveraging the real world," in *Proc. IEEE/CVF Conf. Comput. Vis. Pattern Recognit.*, 2020, pp. 11167-11176.
- [20] S. Huang, Z. Gojcic, Z. Wang, et al., "Neural LiDAR fields for novel view synthesis," in *Proc. IEEE Int. Conf. Comput. Vis. (ICCV)*, 2023.
- [21] T. Tao, L. Gao, G. Wang, et al., "LiDAR-NeRF: Novel LiDAR view synthesis via neural radiance fields," in *Proc. IEEE/CVF Conf. Comput. Vis. Pattern Recognit.*, 2023.
- [22] Lee, Seungjae, Hyungtae Lim, Hyun Myung, et al., "Patchwork++: Fast and robust ground segmentation solving partial under-segmentation using 3D point cloud." in *Proc. 2022 IEEE/RSJ International Conference on Intelligent Robots and Systems (IROS)*. IEEE, 2022.
- [23] OD Team, "OpenPCDet: An open-source toolbox for 3D object detection from point clouds," 2020.
- [24] A. H. Lang, S. Vora, H. Caesar, L. Zhou, J. Yang, and O. Beijbom, "PointPillars: Fast encoders for object detection from point clouds," in *Proc. IEEE Conf. Comput. Vis. Pattern Recognit.*, 2019.